Applied Catalysis B: Environmental 96 (2010) 169–175

Contents lists available at ScienceDirect

Applied Catalysis B: Environmental

journal homepage: www.elsevier.com/locate/apcatb

Study of active sites and mechanism for soot oxidation by silver-loaded ceria catalyst

Ken-ichi Shimizu*, Hiroshi Kawachi, Atsushi Satsuma

Department of Molecular Design and Engineering, Graduate School of Engineering, Nagoya University, Nagoya 464-8603, Japan

ARTICLE INFO

Article history:
Received 27 October 2009
Received in revised form 8 February 2010
Accepted 9 February 2010
Available online 16 February 2010

Keywords:
Ceria
Diesel soot
Oxidation
Silver

ABSTRACT

The catalytic behaviors of metal oxides and Ag-loaded CeO_2 have been studied for soot oxidation by O_2 in tight contact condition. Ag_2O, as the most active oxide among 30 kinds of metal oxides tested, showed high activity even under inert atmosphere. However, Ag_2O completely deactivated after the first catalytic run because of its conversion to Ag metal particle, indicating that Ag_2O does not act as a catalyst but as a strong oxidant for soot combustion. Ag(20 wt%)-loaded CeO_2 (Ag20Ce), consisted of silver metal nanoparticles on CeO_2, showed higher activity than CeO_2, and the catalyst showed high durability. Kinetic studies for soot oxidation under O_2 and He showed that the activation energy changed in the order $CeO_2 > Ag_2O \approx$ Ag20Ce, and activation energy under O_2 was close to those under He, indicating that surface oxygen plays an important role in catalytic soot oxidation in the presence of O_2 and active oxygen species of Ag20Ce and Ag_2O have similar nature. Time-resolved UV–vis analysis of Ce^{4+}/Ce^{3+} redox kinetics under reducing (H_2) and oxidizing (O_2) atmosphere showed that the presence of Ag on CeO_2 enhanced the reduction of Ce^{4+} to Ce^{3+} but did not enhance the re-oxidation of Ce^{3+}. It is concluded that a strong interaction between supported silver nanoparticle and CeO_2 surface results in the formation of highly reducible surface oxygen at silver-ceria interface, whose reactivity for soot oxidation is similar to the surface oxygen of Ag_2O.

1. Introduction

Diesel particle filters are effective for removal of soot (small-size carbon particle) from diesel engine exhausts. The trapped soot in the filters has to be removed continuously or periodically by combustion. The direct oxidation of this soot needs high temperatures (around 600 °C). The high temperature regeneration of the un-catalyzed filter generally carried out by injecting a diesel fuel into the exhaust. This strategy leads to an uncontrolled exotherm, which can destroy a filter. A catalyzed soot oxidation is the way to decrease the soot burn-off temperature in a controlled fashion, and, thereby, increasing the overall fuel efficiency of the diesel engine [1]. To date, many catalyst systems such as transition metal oxides [2–7], precious metals [8,9], and ceria- or lanthanides-based catalysts [9–27] have been reported [1]. However, design concept of soot oxidation catalysts is lacking, because not many fundamental studies are reported in the literature.

Cerium oxides have been fundamentally studied for automotive three-way catalysis, and it is established that its oxygen-storage capacity due to redox between Ce^{4+} and Ce^{3+} under an oxidizing or reducing atmosphere [28–38]. For the soot oxidation by rare earth modified CeO_2 and PrO_x, Makkee and co-workers [17] concluded that the active species should not be lattice oxygen but the adsorbed active oxygen species possibly peroxide or superoxide which spillover onto the soot surface and thereby lowering the on-set temperature of the soot oxidation. Based on the transient kinetic study of soot oxidation with CeO_2 using labeled oxygen, the same group showed that the reduction of CeO_2 lattice oxygen by soot results in the formation of vacant sites which are then filled with gas-phase O_2 [10], and it was proposed that a redox cycle is taking place during the catalytic soot oxidation by CeO_2. Recently, Machida et al. [18] carried out ESR and $^{18}O_2$ pulse reaction studies for soot oxidation by CeO_2. They concluded that the reactive oxygen (superoxide) formed from gaseous O_2 is adsorbed at the three-phase boundary between soot, reduced CeO_2, and the gas phase, but another active oxygen species, which is formed from the lattice oxygen at the CeO_2/soot interface, contributes much more to the total soot oxidation. From the fundamental viewpoint, further study is necessary to reveal the roles of lattice oxygen and redox cycle of CeO_2 in soot oxidation. In addition, there is a contradiction in the effect of metal additives on the soot oxidation activity of CeO_2. Aneggi et al. [9] reported the first systematic study on the effect of silver addition on the soot

* Corresponding author. Fax: +81 52 789 3193.
E-mail address: kshimizu@apchem.nagoya-u.ac.jp (K.-i. Shimizu).

0926-3373/$ – see front matter © 2010 Elsevier B.V. All rights reserved.
doi:10.1016/j.apcatb.2010.02.016

oxidation activity of various metal oxides (CeO_2, ZrO_2, Al_2O_3). They showed that in the case of CeO_2 the addition of silver has little benefit. On the other hand, Machida et al. [18] showed that silver loading onto CeO_2 enhanced the catalytic activity for soot oxidation because of the enhanced generation of superoxide.

Several experimental techniques have been used to study the reduction of Ce^{4+} species in CeO_2-based catalysts: gravimetry, TPR, FTIR, ESR, XPS, and UV–vis [28–34]. However, few studies have succeeded in the in situ dynamic observation of the reduction/re-oxidation processes [35–38]. The direct observation of these processes was recently shown by Yamomoto et al. using in situ time-resolved XAFS [38]. Knowing the previous result by Lavalley and co-workers [32,33] that the intensity of the band in the UV–vis spectrum varied with the degree of reduction, we adopted the in situ diffuse reflectance UV–vis as a convenient method for the in situ characterization of the Ce^{4+}/Ce^{3+} redox processes on CeO_2. To our knowledge, there is no time-resolved UV–vis spectroscopic study on the kinetic analysis of the reduction/re-oxidation processes on the ceria surface [39].

In the present study, through screening tests of various metal oxides, we show that Ag/CeO_2 is highly effective catalyst for soot oxidation. First, we present results for the preparation and XAFS characterization of Ag/CeO_2 with different Ag loading, and then catalytic and kinetics studies of these materials for soot oxidation. Next, the reduction/re-oxidation processes of ceria surface are monitored by in situ time-resolved UV–vis spectroscopy under reducing (H_2) an oxidizing (O_2) atmosphere. The results provide information about the key factors that control the catalytic activity of these materials for soot oxidation.

2. Experimental

2.1. Catalyst preparation

CeO_2 with high surface area (JRC-CEO-1, 157 $m^2\,g^{-1}$) supplied from Catalysis Society of Japan was used as a support material of Ag/CeO_2 catalysts. Ag/CeO_2 catalysts (Ag loading = 1, 5, 10, 20 wt%) were prepared by impregnating support oxides with an aqueous solution of silver nitrate followed by evaporation to dryness at 80 °C, calcination in air at 600 °C for 3 h. The catalyst name is designated as Ag*x*Ce, where *x* is the Ag loading (wt%). Well-calcined metal oxides with surface area of less than 10 $m^2\,g^{-1}$ were commercially purchased and were used for the experiments in Fig. 3. CeO_2 with high surface area (115 $m^2\,g^{-1}$) was prepared by calcination of CeO_2 (JRC-CEO-1) at 500 °C for 3 h.

2.2. XAFS

Ag K-edge XAFS measurements were performed in transmission mode at the BL01B1 in the SPring-8 (Proposal No. 2007A1224, 2008A1633). The storage ring was operated at 8 GeV. A Si(1 1 1) single crystal was used to obtain a monochromatic X-ray beam. Samples were sealed in cells made of polyethylene under ambient atmosphere and XAFS spectra were taken at room temperature. The analysis of the extended X-ray absorption fine structure (EXAFS) was performed using the REX version 2.5 program (RIGAKU). The Fourier transformation of the k^3-weighted EXAFS oscillation from *k* space to *r* space was performed over the range 40–140 nm^{-1} to obtain a radial distribution function. The inversely Fourier filtered data were analyzed with a usual curve fitting method in the *k* range of 40–140 nm^{-1}. For the curve-fitting analysis, the empirical phase shift and amplitude function for the Ag–Ag shell was extracted from the data for Ag foil.

2.3. In situ UV–vis

Diffuse reflectance UV–vis spectra were recorded with UV–vis spectrometer (JASCO V-550) equipped with an in situ flow cell. A diffuse reflectance sample cell is connected with a gas flow system. The light source is led to the center of an integrating sphere by optical fiber. Reflectance was converted to pseudo-absorbance using Kubelka–Munk function. $BaSO_4$ was used to collect a background spectrum. A flow of He was fed to the sample (30 mg) at a flow rate of 100 $cm^3\,min^{-1}$, and UV–vis spectra were recorded at 200–550 °C.

2.4. Catalytic soot oxidation

The catalytic activity for soot oxidation was determined using commercially available carbon black powders (Mitsubishi Chemical Corporation, MA7; surface area 115 $m^2\,g^{-1}$, average particle size 24 nm) as model diesel soot. The soot and catalyst with a weight ratio of 1/80 were ground for 5 min to obtain so-called tight-contact mixtures. Note that the soot/catalyst weight ratio of 1/80 was adopted to avoid a thermal runaway reaction, which occurs when the soot/oxide ratio is relatively large [3]. The catalytic test was carried out with gravimetric thermal analysis (TG/DTA, Rigaku 8120). The soot/catalyst mixture (10 mg) was heated from room temperature to 600 °C at a rate of 5 °C min^{-1} in a stream of 20% O_2 balanced with N_2 (100 $cm^3\,min^{-1}$). The temperature which gives maximum intensity of the exothermic DTA peak (T_{max}) was used to compare soot oxidation activity of different catalyst. The effluent gas was analyzed by nondispersive infrared (NDIR) CO/CO_2 analyzers (Horiba VIA510).

The apparent activation energy of the soot oxidation is determined by the Ozawa method [17] using the following expression:

$$\mathrm{d}\,\log(\beta)/\mathrm{d}(1/T_\alpha) = 0.4567\,E/R$$

where β is the heating rate used, T_α the temperature corresponding to α% carbon conversion, *E* is the apparent activation energy in kJ mol^{-1}. *E* can be estimated from the slope of the least squares straight line fit of $\log(\beta)$ versus $1/T_\alpha$ plot.

3. Results and discussion

3.1. Characterization of Ag/CeO_2

To investigate the structure of Ag species, Ag K-edge X-ray absorption fine structure (XAFS) measurement of Ag/CeO_2 and Ag reference compounds was carried out. Fig. 1A shows the Fourier transforms of the k^3-weighted Ag K-edge extended X-ray absorption fine structure (EXAFS) of Ag/CeO_2 catalysts with various Ag loading (5, 10, 20 wt%). For all the catalysts, the peak at 1.6 Å due to the nearest oxygen atoms are absent, while the peak at 2.6 Å due to the scattering from the nearest silver atoms in metallic silver are clearly observed. The intensity of the peak due to Ag-Ag contribution of these catalysts are lower than that of silver powder, suggesting that metallic silver species in these catalysts are small nanoparticles. The intensity of the Ag–Ag peak increased with silver loading, which suggests that the particle size of metallic silver increases with silver loading. The structural parameters derived from curve-fitting analysis are listed in Table 1. The EXAFS of Ag5Ce, Ag10Ce, and Ag20Ce showed an Ag–Ag shell with coordination number of 5.3–9.8 and bond distance of 2.89 Å. The Ag–Ag distance is the same as that of bulk Ag, indicating the presence of metallic silver. The Ag–Ag coordination numbers (5.0–9.8) were lower than that of bulk Ag (12). These results indicate that small metal nanoparticles are the dominant silver species in these catalysts.

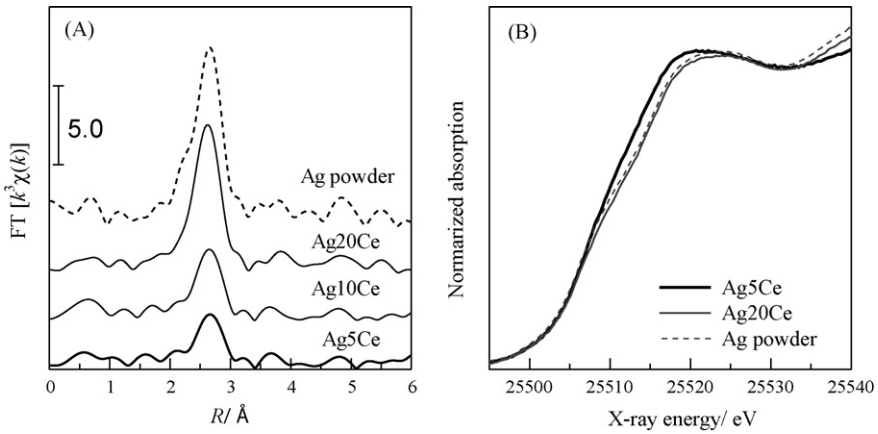

Fig. 1. Ag K-edge EXAFS Fourier transforms (A) and XANES spectra (B) of Ag/CeO_2 samples and a reference sample (Ag powder).

The Ag–Ag coordination number increased with an increase in Ag loading, indicating that mean size of silver nanoparticles increases with silver loading. Fig. 1B shows Ag K-edge X-ray absorption near-edge structures (XANES) spectra, which are known to be sensitive to the oxidation state of X-ray absorbing atom. The XANES feature of AgCe20 is similar to that of Ag powder, indicating that silver species in these samples are in a reduced state. On the other hand, the XANES feature of AgCe5 slightly differs from that of Ag powder; a weak peak centered around 25518 eV due to Ag^+ species [40] is observed. Combined with the EXAFS result of Ag5Ce, which indicates that small metal nanoparticles are the dominant silver species in Ag5Ce, it is concluded that Ag5Ce consists of Ag metal nanoparticles as dominant Ag species together with Ag^+ species as minor Ag species. This model is qualitatively the same as shown by Aneggi et al. [9]. Their high-resolution transmission electron microscopy showed that both Ag metal particle and Ag_2O were present on 5 wt%Ag/CeO_2. However, their conclusion is quantitatively different from our model. They showed that the silver in a positive oxidation state is favored with CeO_2. This is different from our structural model. The difference may be due to a difference in the CeO_2 source: CeO_2 used in this study has higher surface area (157 $m^2\,g^{-1}$) than that in ref. [9] (49 $m^2\,g^{-1}$).

3.2. Carbon oxidation

First, soot oxidation activity of various metal oxides (MO_x: M = Ag, Ce, Mn, Bi, La, Er, Mo, Fe, Gd, Ni, Tb, Dy, Y, In, Ho, Sm, Sn, Yb, Nb, Ta, Al, Ti, Ga) was evaluated by exothermal change in DTA profile and produced CO_2 in gas phase. Typical DTA and CO_2 emission profiles for Ag_2O and CeO_2 versus reaction temperature are shown in Fig. 2. For the results in Fig. 2, CO_2 was a sole product, and CO formation was negligible. As shown in Fig. 2B, the DTA profile of Ag_2O showed the largest exothermal peak at 206 °C and two weak peaks at 257 °C and above 300 °C. The CO_2 emission profile of Ag_2O showed similar features: the largest peak at 211 °C and two weak peaks at 264 °C and above 300 °C. For CeO_2 catalyst (Fig. 2A), the CO_2 emission profile exhibiting a maximum intensity at 369 °C and the DTA profile exhibiting a maximum intensity at 360 °C are very similar to each other. Thus, we used the temperature for the maximum intensity of the exothermic DTA peak (T_{max}) as a parameter to compare the soot oxidation activity of different catalyst. In order to study the effect of metal-oxygen bond strength of metal oxide catalysts on the soot oxidation activity, the temperature which gives the maximum DTA value in exothermic DTA curve (T_{max}) is plotted in Fig. 3 as a function of the enthalpy of formation of bulk oxide ($-\Delta H_f$) [41]. Note that the oxides tested were well-calcined commercial samples with surface area below 10 $m^2\,g^{-1}$ except for the CeO_2 with surface area of 115 $m^2\,g^{-1}$ (from Fig. 2A). Among the oxides tested, Ag_2O showed the lowest T_{max} value, which indicate that Ag_2O showed the highest activity for soot oxidation.

Table 1
Ag K-edge EXAFS analysis of various catalysts.

Catalysts	Shell	CN[a]	R/Å[b]	(σ^2)/Å^2[c]	R_f/%[d]
Ag5Ce	Ag	5.3	2.89	0.076	2.2
Ag10Ce	Ag	6.2	2.89	0.071	1.9
Ag20Ce	Ag	9.8	2.89	0.061	1.4

[a] Coordination numbers.
[b] Bond distance.
[c] Debye–Waller factor.
[d] Residual factor.

When the metal oxide with low $-\Delta H_f$ is once converted to metallic species, its re-oxidation is more difficult than the metal oxides with high $-\Delta H_f$. It follows that the metal oxides with low $-\Delta H_f$ value cannot act as catalyst for soot oxidation when the oxide is once thermally decomposed or reduced by carbon during the soot oxidation. Actually, XRD results showed that Ag_2O completely changed to Ag metal after the first soot oxidation experiment (result not shown). When the second soot oxidation was performed using the same catalyst powder, T_{max} of Ag_2O was increased from 206 °C to 469 °C (Fig. 2B, dashed lines). In contrast, CeO_2 as a metal oxide with moderate $-\Delta H_f$, was thermally more stable; T_{max} value of 357 °C in the DTA profile for the second soot oxidation test (Fig. 2A, dashed lines) was not higher than that for the first run (360 °C).

As shown in Fig. 3, the T_{max} value of CeO_2 markedly decreased (from 468 to 360 °C) with an increase in the surface area (from 4.7 to 115 $m^2\,g^{-1}$). Hereafter, the CeO_2 catalyst with high surface area, whose soot oxidation profiles are shown in Fig. 2A, was used as a standard CeO_2 catalyst as well as for the support material of Ag/CeO_2 catalysts. Fig. 2C shows DTA and CO_2 emission profiles of the Ag/CeO_2 catalyst with Ag loading of 20 wt% (Ag20Ce). Loading of 20 wt% silver resulted in an improvement in soot oxidation activity of CeO_2. The T_{max} value in the DTA profile of Ag20Ce in the first run (266 °C) was 94 °C lower than that of CeO_2 in the first run (360 °C). Although T_{max} value shifted to higher temperature in the second run (308 °C), this value was still lower than that of CeO_2 (357 °C).

Fig. 4 shows the effect of Ag loading on the T_{max} value for the soot oxidation with Ag/CeO_2 catalysts. T_{max} gradually decreased with an increase in the silver loading. The activation energy (E) for the Ag/CeO_2 catalyzed soot oxidation reaction was estimated by a well-established method in the literature [17]. Fig. 5 shows an example of analytical procedure for Ag5Ce. The soot oxidation experiments under the standard condition were carried out at different heating rates (β = 1, 3, 5, 10 °C min^{-1}). The plots of the logarithmic heating

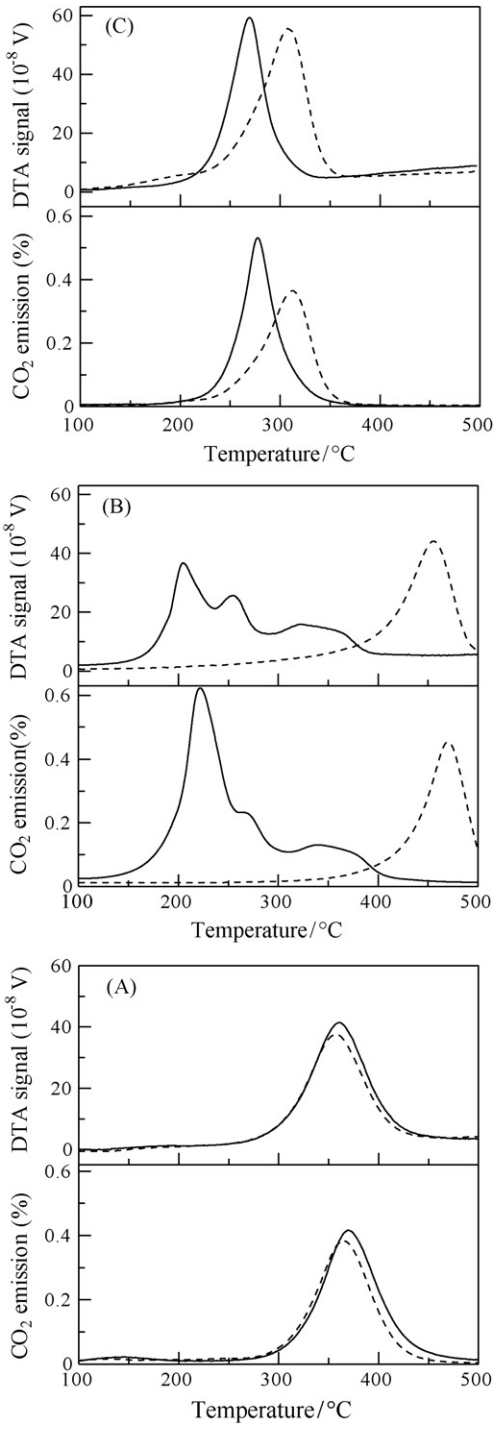

Fig. 2. Profiles of DTA and CO_2 emission for carbon oxidation with (solid lines) fresh catalysts and (dashed lines) reused catalysts: (A) CeO_2, (B) Ag_2O, and (C) Ag20Ce. Conditions: soot/catalyst = 1/80(w/w), heating rate = 5 °C min^{-1}, 20% O_2/N_2 flow (100 cm^3 min^{-1}), tight contact.

rates ($\log\beta$) versus the inverse temperatures ($1/T_\alpha$) at the various soot conversion levels (α = 10%, 20%, 30%, 40%, 50%, 60%, and 70%) showed good linear fits. The E value estimated from the slope of the T_{10} plot is 106 kJ mol, which is identical to the average E value (106 ± 4 kJ mol^{-1}) estimated from the slopes of all plots in Fig. 5. Such experiments were carried out for all the Ag/CeO_2 catalysts. E values for the catalysts with different silver loading (0, 1, 5, 10, 20 wt%) are shown Fig. 4. The activation energy for the CeO_2-catalyzed carbon oxidation is 126 kJ mol^{-1}. Modification of

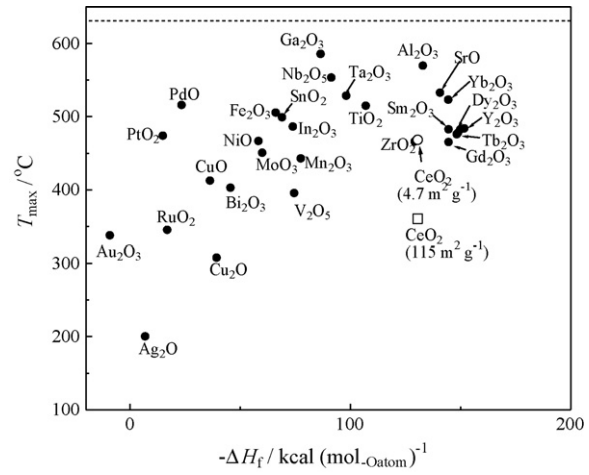

Fig. 3. Plot of T_{max} for carbon oxidation versus enthalpy of formation of bulk oxide catalysts. A dashed line denotes T_{max} for carbon oxidation without catalyst.

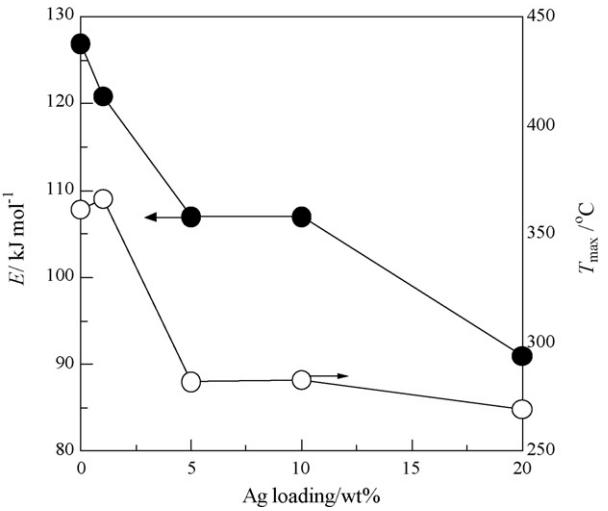

Fig. 4. Activation energy and T_{max} for carbon oxidation as a function of Ag loading of Ag/CeO_2 catalysts.

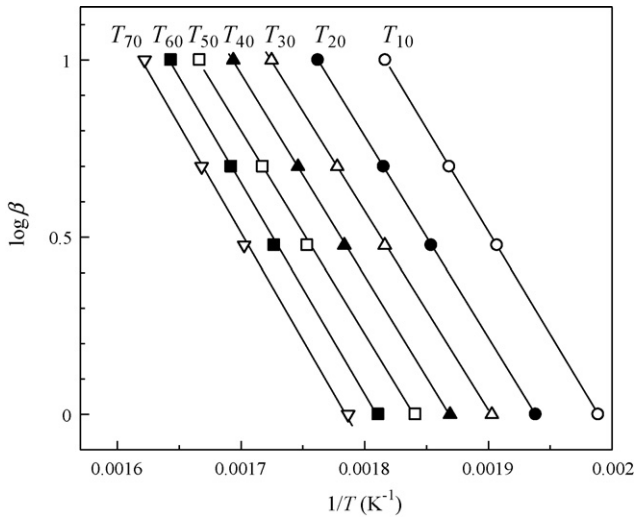

Fig. 5. Ozawa plots over Ag5Ce at different carbon conversion levels (α) for carbon oxidation with heating rates (β) of 1, 3, 5, and 10 K min^{-1}. T_α denotes the temperature at α% conversion.

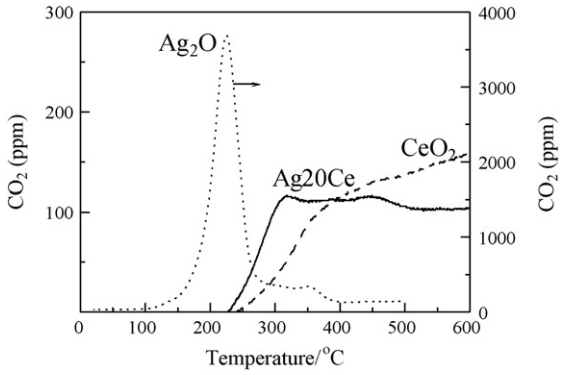

Fig. 6. CO_2 formation profiles during temperature programmed carbon oxidation with various catalysts under flowing He. Heating rate: 10 °C min^{-1} for Ag20Ce and CeO_2, 5 °C min^{-1} for Ag_2O.

the CeO_2 surface with 5–10 wt% of Ag resulted in a decrease in the activation energy to 106 kJ mol^{-1}, and the activation energy was lowest for the Ag/CeO_2 catalyst with 20 wt% silver loading (92 kJ mol^{-1}). Combined with the EXAFS results, the above results indicate that modification of CeO_2 with metallic Ag nanoparticles markedly improves the soot oxidation activity of CeO_2, and the addition of metallic Ag nanoparticles results in a decrease in the activation energy of the rate determining step or a change in the rate determining step. In a separate set of experiments, the activation energy for the soot oxidation with Ag_2O was estimated in the same manner as in Fig. 5. The activation energy of Ag20Ce (92 kJ mol^{-1}) was rather close to that of Ag_2O (78 kJ mol^{-1}) but lower than that of CeO_2 (126 kJ mol^{-1}). This result suggests that the active oxygen species of Ag20Ce have similar nature to those of Ag_2O.

Concerning the reaction mechanism for carbon oxidation by transition metal oxides such as CeO_2, several authors pointed out the importance of redox properties of the catalyst. That is, the effectiveness of the catalyst can be related to its ability to deliver oxygen from the lattice to the surface of carbon. Makkee and co-workers established that the role of CeO_2 in carbon oxidation is to cause spillover of active oxygen from CeO_2 onto the soot surface and its subsequent adsorption at the active carbon site is an important step in the carbon oxidation mechanism [17]. Machida et al. [18] have studied the reasons why CeO_2 is an active catalyst for carbon oxidation and showed a marked contribution of the surface-active oxygen species formed from the lattice oxygen of CeO_2 in the carbon oxidation. To evaluate the effect of silver on the reactivity of the surface oxygen of CeO_2 in the carbon oxidation, we measured the CO_2 formation from the carbon/catalyst tight-contact mixtures in flowing He. The sample was first heated up to 220 °C at a rate of 10 °C min^{-1}, followed by purging the sample under He for 30 min. Then, the sample was heated to 600 °C at different heating rates (β). Fig. 6 illustrates CO_2 formation profiles in a temperature range of 220–600 °C for Ag20Ce (β = 10 °C min^{-1}), CeO_2 (β = 10 °C min^{-1}) and Ag_2O (β = 5 °C min^{-1}). Note that CO_2 was a sole product but CO was negligible. Ag20Ce showed higher activity for soot oxidation under He than CeO_2 at low temperature region (below 400 °C). To estimate the activation energy under He (E_{He}), the experiments in Fig. 6 were carried out at different heating rates (β = 10, 20, 30, 40 °C min^{-1} for Ag20Ce, CeO_2 and β = 1, 3, 5, 10 °C min^{-1} for Ag_2O). The plots of the logarithmic heating rates (log β) versus the inverse temperatures at which 10% of soot is converted to CO_2 ($1/T_{10}$) showed good linear fits (not shown). The E_{He} value estimated from the slope of the plot are summarized in Table 2, together with the activation energy for the standard soot oxidation under 20% O_2 (E). For each catalysts, the activation energy for soot oxidation under 20% O_2 is very close to the value under He, which suggests that surface oxygen plays an important role in catalytic soot oxidation in the presence of O_2. The E_{He} value of Ag20Ce (85 kJ mol^{-1}) was close to that of Ag_2O (81 kJ mol^{-1}) but much lower than that of CeO_2 (126 kJ mol^{-1}), indicating that the nature of the active oxygen species on Ag20Ce is rather similar to that on Ag_2O.

Table 2
Apparent activation energies of soot oxidation under 20% O_2/N_2 (E) or under He (E_{He}) over various catalysts and activation energies for Ce^{4+} reduction in 0.5% H_2 (E_{Rd}) and Ce^{3+} re-oxidation in 10% O_2 (E_{Ox}) from Fig. 9.

Catalysts	E (kJ mol^{-1})	E_{He} (kJ mol^{-1})	E_{Rd} (kJ mol^{-1})	E_{Ox} (kJ mol^{-1})
CeO_2	126	126	120	81
Ag_2O	77	81	–	–
Ag20Ce	92	85	15	22

3.3. In situ UV–vis experiments

Diffuse reflectance UV–vis spectroscopy has been used for characterizing Ce^{3+} species formed by the reduction of CeO_2 with H_2 [32,33]. It is well established that the band around 600–750 nm corresponds to Ce^{3+} to Ce^{4+} charge-transfer interactions and can be used to follow the variation of the reduction degree of ceria. For a kinetic analysis of the reduction/re-oxidation processes on the ceria surface, we adopted a time-resolved in situ diffuse reflectance UV–vis spectroscopy [39]. The reduction of the lattice oxygen on the ceria surface under 0.5% H_2 flow and subsequent re-oxidation under 10% O_2 were used as test reactions. UV–vis spectra of Ag5Ce after pre-oxidation with 10% O_2/He at 250 °C and after subsequent reduction with 0.5% H_2/He for are shown in Fig. 7A. After the pre-oxidation, only a cerium to oxygen charge transfer band centered around 400 nm was observed. When Ag5Ce was reduced with H_2, a broad band in a range 500–800 nm due to Ce^{3+} to Ce^{4+} charge-transfer interactions appeared. This indicates that surface Ce^{4+} species in this sample were reduced to Ce^{3+} species with H_2, accompanying a removal of the lattice oxygen on the surface of CeO_2 support. A subtraction of the spectrum after the reduction by the spectrum before the reduction yields a difference spectrum shown in Fig. 7B (dashed line).

The reduction of surface Ce^{4+} ions on the Ag5Ce catalyst after the reaction with carbon as a reductant can be monitored by in situ UV–vis. A carbon/Ag5Ce (80 mg/1 mg) tight-contact mixture placed in the in situ UV–vis cell was heated at 600 °C in flowing He for 3 h, and then a spectrum shown in Fig. 7A (dotted line) was taken at 600 °C. A difference spectrum obtained from a subtraction of this spectrum by the spectrum after the pre-oxidation is shown in Fig. 7B. A broad band in a range 500–800 nm due to Ce^{3+} to Ce^{4+} charge-transfer interactions appeared, which indicates that surface Ce^{4+} species in this sample were reduced by carbon to Ce^{3+} species. Note that the absence of carbon in the Ag5Ce sample after this UV–vis experiment was confirmed by DTA analysis. Hence the band above 600 nm is not due to residual carbon but due to Ce^{3+}. The above results indicate that the lattice oxygen of ceria surface (surface Ce^{4+}-O site) in the AgCe5 catalyst is consumed by its reaction with carbon to yield Ce^{3+} ion and adjacent oxygen vacancy site on the catalyst surface and CO_2.

For the in situ UV–vis results on the H_2-reduction of Ag5Ce and CeO_2 samples, changes in heights of the band at 750 nm in the difference spectrum at 400 °C are plotted as a function of H_2-reduction time in Fig. 8. It is shown that the rate of Ce^{4+} reduction estimated from the slope of the line is higher for Ag5Ce than CeO_2. After the steady-states, the flowing gas was switched from 0.5% H_2 to 10% O_2, and a decrease in the intensity of the band due to Ce^{3+} was observed. The relative rate of Ce^{3+}-oxidation estimated from the slope of the curve is higher for CeO_2 than Ag5Ce. Similar sets of experiments were performed for these samples at different temperatures: in a

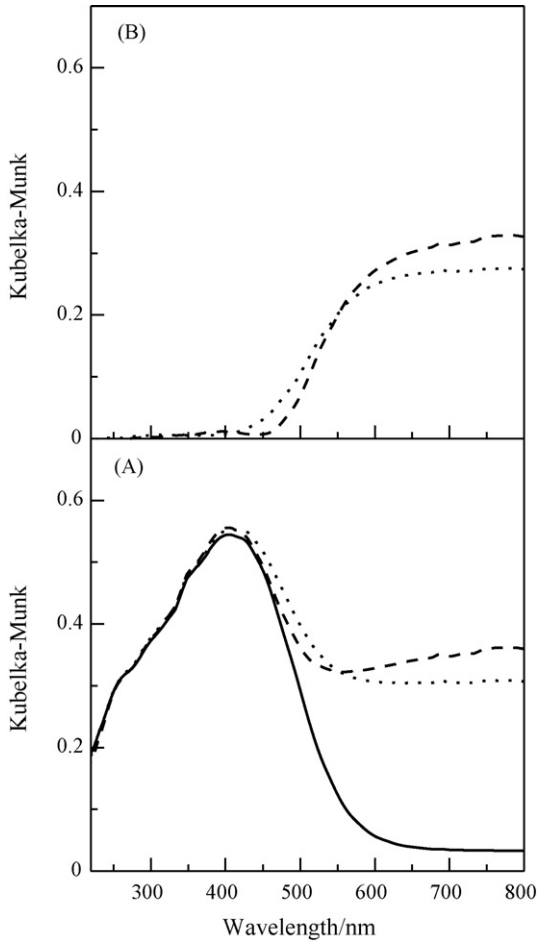

Fig. 7. (A) In situ diffuse reflectance UV–vis spectra of Ag5Ce: (solid line) after pre-oxidation in 10% O_2/He for 0.5 h at 600 °C followed by purging with He for 10 min at 250 °C, (dashed line) after the reduction by 0.5% H_2/He at 250 °C for 20 min, and (dotted line) after the reduction by carbon at 600 °C for 180 min (catalyst:carbon = 80 mg:1 mg). (B) Difference spectra.

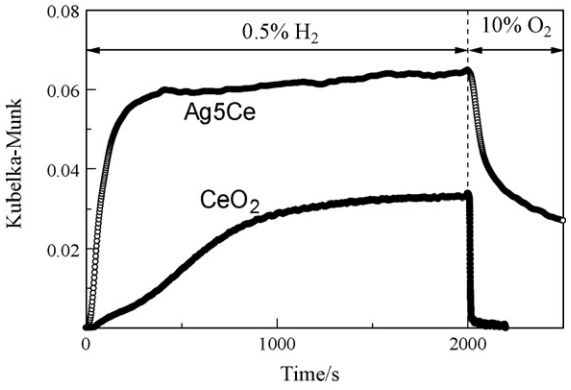

Fig. 8. Charges in the intensity at 750 nm for UV–vis spectra of (○) Ag5Ce and (●) CeO_2 at 400 °C. Samples were first reduced by 0.5% H_2/He (t = 0–2000 s) and then re-oxidized under 10% O_2/He (t > 2000 s).

range 200–400 °C for Ag5Ce and in a range 400–550 °C for CeO_2. The rates of Ce^{4+} reduction to Ce^{3+} with H_2 and Ce^{3+} re-oxidation to Ce^{4+} with O_2 for both samples are plotted in Fig. 9 as Arrenius plots. The activation energies for Ce^{4+} reduction (E_{Rd}) and Ce^{3+} re-oxidation (E_{Ox}) were estimated from the slope of the lines and listed in Table 2. It is found that the loading of silver nanoparticles on CeO_2 resulted in a significant decrease in the activation energies for Ce^{4+} reduction (from 120 to 15 kJ mol^{-1}) and Ce^{3+} re-oxidation (from 81 to 22 kJ mol^{-1}). This indicates that both reduction and re-oxidation of CeO_2 surface is promoted by silver nanoparticles. However, the loading of Ag nanoparticles on CeO_2 should result in a decrease in the number of the exposed CeO_2 surface, and this can be a possible reason of the lower rate of Ce^{3+} re-oxidation for Ag5Ce than CeO_2 (Fig. 8). It is concluded that the silver nanoparticle enhances reducibility of CeO_2 under H_2, while it does not enhance the re-oxidation of reduced CeO_2 surface by O_2 under the condition adopted in this study.

From the above discussions, we propose a possible reaction mechanism of carbon oxidation by Ag/CeO_2 catalysts in Fig. 10. First, gas-phase O_2 is chemisorbed on the oxygen vacancy site adjacent to Ce^{3+} ion and silver nanoparticle to yield reactive oxygen species (O_n^{x-}) having a similar reducibility as the lattice oxygen of Ag_2O. The reactive oxygen species, which may migrate to the surface of carbon, oxidize it to CO_2, accompanying by the re-production of Ce^{3+} ion and adjacent oxygen vacancy site at silver-ceria interface. Taking into account the previous report that O_2^- was observed in thermally decomposed silver oxides [42], we believe that the most probable candidate of the reactive oxygen species is O_2^- proposed by Machida et al. [18] for CeO_2 and Ag/CeO_2 catalyst for soot oxidation. Uner et al. [5] showed TG result for soot oxidation by CoO*x*-PbO*x* catalyst with soot/catalyst ratio of 1/9. They showed that significant amounts of CO were detected when oxygen was completely depleted in the gas phase [5]. In contrast, when soot/Ag20Ce mixture with soot/catalyst ratio of 1/4 is heated at a rate of 20 °C min^{-1} from 220 to 600 °C in flowing He, CO_2 was a sole product but CO formation was below 3 ppm (result not shown). There are two possible explanation which account for this result. One is that carbon is oxidized by a reactive oxygen species as atomic oxygen species and CO intermediate reacts immediately

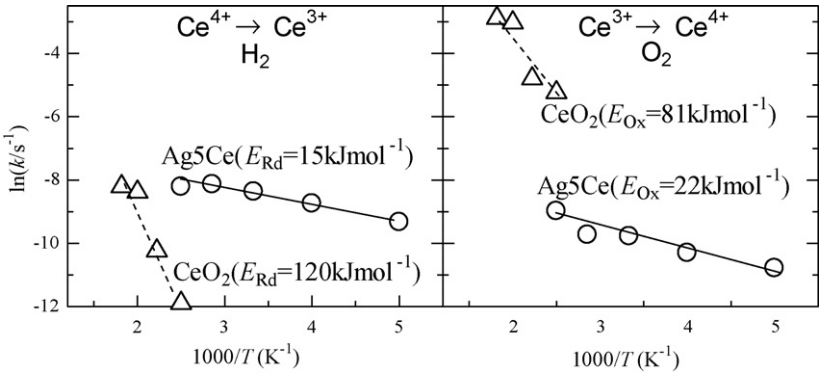

Fig. 9. Arrenius plots for (left) reduction of Ce^{4+} to Ce^{3+} with 0.5%H_2 and (right) re-oxidation of Ce^{3+} to Ce^{4+} with 10%O_2 over (circles) Ag5Ce and (triangles) CeO_2. Apparent activation energies determined from the plots are in the parentheses.

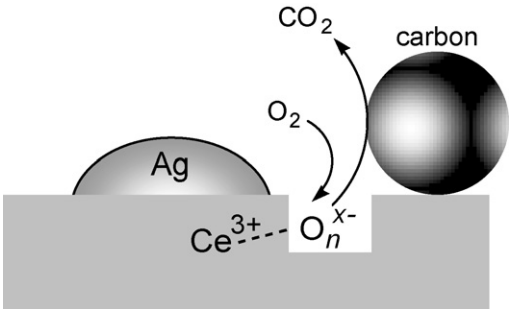

Fig. 10. Schematic mechanism of soot oxidation over Ag/CeO_2 catalyst.

with another reactive oxygen species to produce CO_2. The other explanation is that carbon is oxidized by the reactive molecular species such as O_2^- to produce CO_2. At present it is difficult to conclude which is more favorable model. Thus, we tentatively denote O_n^{x-} ($n = 1$ or 2, $x = 1$ or 2) as a possible reactive oxygen species in Fig. 10. Instead of the mechanism in Fig. 10, one may assume that two different soot oxidation mechanisms account for the present experimental results: on one hand the redox route of ceria and on the other hand a mechanism correlated to the capability of silver to form oxide. However, the good linearity in the plot of the logarithmic heating rates ($\log \beta$) versus the inverse temperatures in Fig. 5 suggests that there is one mechanism for Ag/CeO_2-catalyzed soot oxidation in the present condition.

4. Conclusions

Among the 30 kinds of metal oxides tested, Ag_2O is found to be the most reactive metal oxide. However, Ag_2O acts as a stoichiometric oxidant for soot combustion and converted to the uncreative metallic silver after the reaction. In contrast, CeO_2 as a metal oxide with moderate reducibility was thermally stable. Loading of silver metal nanoparticles on CeO_2 significantly improves the reactivity of CeO_2 lattice oxygen in the soot oxidation under an inert atmosphere as well as the catalytic activity of CeO_2 for soot oxidation by O_2. Kinetic studies for the soot oxidation indicate that the CeO_2 lattice oxygen interacted with silver nanoparticle has similar reactivity to the lattice oxygen of Ag_2O. The silver nanoparticle also enhances reducibility of CeO_2 under H_2, while it does not enhance the re-oxidation of reduced CeO_2 surface by O_2 under the condition adopted in this study. It is concluded that reducibility of the lattice oxygen of CeO_2 is enhanced by an adjacent silver nanoparticle, which results in the enhanced catalytic activity for soot oxidation.

Acknowledgments

This work was partly supported by a Grant-in-Aid for Scientific Research B (20360361) from the Japan Society for the Promotion Science. The X-ray absorption experiment was performed with the approval of the Japan Synchrotron Radiation Research Institute (Proposal No. 2007A1224).

References

[1] B.A.A.L. van Setten, M. Makkee, J.A. Moulijn, Catal. Rev. 43 (2001) 489.
[2] J.P.A. Neeft, M. Makkee, J.A. Moulijn, Appl. Catal. B 8 (1996) 57.
[3] J.P.A. Neeft, F. Hoornaert, M. Makkee, J.A. Moulijn, Thermochim. Acta 287 (1996) 261.
[4] W.F. Shangguan, Y. Teraoka, S. Kagawa, Appl. Catal. B 8 (1996) 217.
[5] D. Uner, M.K. Demirkol, B. Dernaika, Appl. Catal. B 61 (2005) 334.
[6] Y. Teraoka, K. Nakano, S. Kagawa, Appl. Catal. B 34 (2001) 73.
[7] J. Liu, Z. Zhao, C. Xu, A. Duan, T. Meng, X. Bao, Catal. Today 119 (2007) 267.
[8] J. Oi-Uchisawa, A. Obuchi, S. Wang, T. Nanba, A. Ohi, Appl. Catal. B 43 (2003) 117.
[9] E. Aneggi, J. Llorca, C. de Leitenburg, G. Dolcetti, A. Trovarelli, Appl. Catal. B 91 (2009) 489.
[10] A. Bueno-López, K. Krishna, M. Makkee, J.A. Moulijn, Catal. Lett. 99 (2005) 203.
[11] T. Masui, K. Minami, K. Koyabu, N. Imanaka, Catal. Today 117 (2006) 187.
[12] T. Ishihara, T. Oishi, S. Hamamoto, Catal. Commun. 10 (2009) 1722.
[13] Q. Liang, X. Wu, X. Wu, D. Weng, Catal. Lett. 119 (2007) 265.
[14] I. Atribak, A. Bueno-López, A. García-Garía, J. Catal. 259 (2008) 123.
[15] E. Aneggi, C. de Leitenburg, G. Dolcetti, A. Trovarelli, Catal. Today 114 (2006) 40.
[16] A. Bueno-López, K. Krishna, B. van der Linden, G. Mul, J.A. Moulijn, M. Makkee, Catal. Today 121 (2007) 237.
[17] K. Krishna, A. Bueno-López, M. Makkee, J.A. Moulijn, Appl. Catal. B 75 (2007) 189.
[18] M. Machida, Y. Murata, K. Kishikawa, D. Zhang, K. Ikeue, Chem. Mater. 20 (2008) 4489.
[19] S.B. Simonsen, S. Dahl, E. Johnson, S. Helveg, J. Catal. 255 (2008) 1.
[20] B. Dernaika, D.A. Uner, Appl. Catal. B 40 (2003) 219.
[21] M.N. Bokova, C. Decarne, E. Abi-Aad, A.N. Pryakhin, V.V. Lunin, A. Aboukaïs, Thermochim. Acta 428 (2005) 165.
[22] A. Bueno-Lopez, K. Krishna, M. Makkee, J.A. Moulijin, J. Catal. 230 (2005) 237.
[23] K. Krishna, A. Bueno-Lopez, M. Makkee, J.A. Moulijn, Appl. Catal. B 75 (2007) 189.
[24] K. Krishna, A. Bueno-Lopez, M. Makkee, J.A. Moulijn, Appl. Catal. B 75 (2007) 201.
[25] K. Krishna, A. Bueno-Lopez, M. Makkee, J.A. Moulijn, Appl. Catal. B 75 (2007) 210.
[26] X. Wu, D. Liu, K. Li, J. Li, D. Weng, Catal. Commun. 8 (2007) 1274.
[27] M.A. Peralta, V.G. Milt, L.M. Cornaglia, C.A. Querini, J. Catal. 242 (2006) 118.
[28] H.C. Yao, Y.F. Yu Yao, J. Catal. 86 (1984) 254.
[29] T. Miki, T. Ogawa, M. Haneda, N. Kakuta, A. Ueno, S. Tateishi, S. Matsuura, M. Sato, J. Phys. Chem. 94 (1990) 6464.
[30] M. Ozawa, M. Kimura, A. Isogai, J. Alloys Compd. 193 (1993) 73.
[31] T. Bunluesin, H. Cordatos, R.J. Gorte, J. Catal. 157 (1995) 222.
[32] A. Laachir, V. Perrichon, A. Badri, J. Lamotte, E. Catherine, J.C. Lavalley, J. El Fallah, L. Hilaire, F. le Normand, E. Quemere, G.N. Sauvion, O. Touret, J. Chem. Soc. Faraday Trans. 87 (1991) 1601.
[33] C. Binet, A. Badri, J.-C. Lavalley, J. Phys. Chem. 98 (1994) 6392.
[34] F. Zhang, P. Wang, J. Koberstein, S. Khalid, S.W. Chan, Surf. Sci. 563 (2004) 74.
[35] Y. Sakamoto, K. Kizaki, T. Motohiro, Y. Yokota, H. Sobukawa, M. Uenishi, H. Tanaka, M. Sugiura, J. Catal. 211 (2002) 157.
[36] J.A. Rodriguez, J.C. Hanson, J.Y. Kim, G. Liu, A. Iglesias-Juez, M. FernLndez-GarcMa, J. Phys. Chem. B 107 (2003) 3535.
[37] J. el Fallah, S. Boujana, H. Dexpert, A. Kiennemann, J. Majerus, O. Touret, F. Villain, F. Le Normand, J. Phys. Chem. 98 (1994) 5522.
[38] T. Yamamoto, A. Suzuki, Y. Nagai, T. Tanabe, F. Dong, Y. Inada, M. Nomura, M. Tada, Y. Iwasawa, Angew. Chem. Int. Ed. 46 (2007) 9253.
[39] F.C. Jentoft, Adv. Catal. 52 (2009) 129.
[40] K. Shimizu, J. Shibata, H. Yoshida, A. Satsuma, T. Hattori, Appl. Catal. B 30 (2001) 151.
[41] D.E. Fein, I.E. Wachs, J. Catal. 210 (2002) 241.
[42] S. Tanaka, T. Yamashita, J. Catal. 40 (1975) 140.